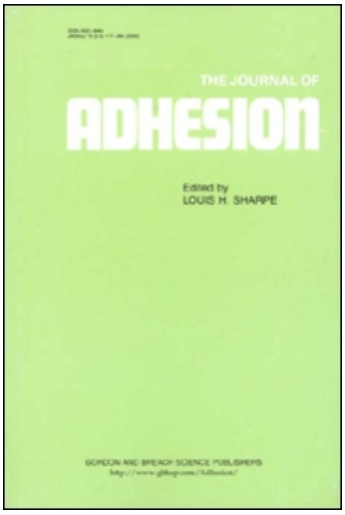

The Journal of Adhesion
Publication details, including instructions for authors and subscription information:
http://www.informaworld.com/smpp/title~content=t713453635

Interfacial Bonding and Environmental Stability of Polymer Matrix Composites

D. H. Kaelble[a]; P. J. Dynes[a]; E. H. Cirlin[a]
[a] North American Rockwell Science Center, California, U.S.A.

To cite this Article Kaelble, D. H. , Dynes, P. J. and Cirlin, E. H.(1974) 'Interfacial Bonding and Environmental Stability of Polymer Matrix Composites', The Journal of Adhesion, 6: 1, 23 — 48
To link to this Article: DOI: 10.1080/00218467408072237
URL: http://dx.doi.org/10.1080/00218467408072237

J. Adhesion, 1974, Vol. 6, pp. 23–48

Printed in Northern Ireland

Interfacial Bonding and Environmental Stability of Polymer Matrix Composites†

D. H. KAELBLE, P. J. DYNES and E. H. CIRLIN

North American Rockwell Science Center Thousand Oaks, California 91360, U.S.A.

(*Received January 8, 1973*)

Recently developed adsorption-interdiffusion (A-I) theory of adhesion is employed to isolate the (London) dispersion γ_{ij}^{d} and (Keesom) polar γ_{ij}^{p} components of the excess interfacial free energy $\gamma_{ij} = \gamma_{ij}^{d} + \gamma_{ij}^{p}$ at the fiber-matrix interface in polymer matrix composites. For adsorption bonded interfaces the theory defines a new method of mapping the surface energy effects of an immersion phase upon the Griffith fracture energy γ_G. The stability of interfacial bonding between graphite fiber-epoxy matrix is defined in terms of the theoretical model and experimentally evaluated by accelerated aging studies which monitor changes in fracture energy for crack propagation perpendicular to the fiber axis. Applications of the model to control fiber surface treatments and select matrix components for optimized bond strength and environmental resistance is discussed.

INTRODUCTION

A better understanding of the relationships between interfacial bonding and environmental stability remains as one of the important areas of research in polymer matrix composites.[1,2] Advanced composites utilize the new high performance boron, graphite, or high modulus organic fibers in place of the traditional glass reinforcement.[3] The transmission of stress between fiber and

† Presented at the Symposium on "Interfacial Bonding and Fracture in Polymeric, Metallic and Ceramic Composites" at The Univ. of California at Los Angeles, Nov. 13–15, 1972. This Symposium was jointly sponsored by the Polymer Group of So. California Section, ACS and Materials Science Department, U.C.L.A.

matrix depends upon a strong interfacial bond that resists failure. In a converse role the preferential failure of the interface during microfracture of a composite may increase fracture toughness by diverting crack growth mechanisms and delocalizing stress at the crack tip.[1] This study forms part of a more general research program in the mechanisms of bonding and fracture in polymeric composite systems whose analysis scheme is outlined in Table I.[4,5] A detailed study of the central subject of this discussion would involve

TABLE I

Outline for detailed analysis of adhesive bonding and failure mechanisms

I. Interfacial chemistry
   a. Adsorption mechanisms of adhesion.
   b. Interdiffusion mechanisms of adhesion.
   c. Ionic-covalent (chemical) mechanisms.
   d. Effects of bond polarity on service life.
II. Rheological factors in the individual phases affecting adhesion and failure.
   a. Chemo-rheological mechanisms.
   b. Viscoelastic mechanisms.
   c. Shear and dilational mechanisms.
III. Mechanics factors of system response.
   a. Critical fracture stresses and energies.
   b. Definition of realistic failure criteria.
   c. Modes of loading.
   d. Definition of realistic thermal, pressure, and stress histories.
   e. Measurement of failure kinetics under realistic histories of separate and combined stress and environmental exposure.
   f. Correlation of data in terms of service life theory.
   g. Correlation of data with nondestructive testing (NDT).

all elements of Table I. It is evident that factors involving interfacial chemistry, rheology, mechanic aspects of response need to be interrelated in more detailed fashion in order to properly define the performance and reliability of reinforced composites subjected to environmental degradation. The symbols and nomenclature for the principal parameters that define the scope of this discussion are presented in Table II.

THEORETICAL CONSIDERATIONS

An extended form of the adsorpton-interdiffusion (A-I) model for interfacial interactions defines a new method of analyzing the surface energy effects of an immersion phase upon the Griffith fracture energy γ_G.[6] The conventional relations for describing the (London-d) dispersion and (Keesom-p) polar interactions between liquids and solids are stated as follows:[4,5]

$$\gamma_{LV} = \gamma_{LV}^{d} + \gamma_{LV}^{p} = \alpha_L^2 + \beta_L^2 \tag{1}$$

$$\gamma_{SV} = \gamma_{SV}^{d} + \gamma_{SV}^{p} = \alpha_S^2 + \beta_S^2 \tag{2}$$

$$\gamma_{SV} = \gamma_{S^o} - \Pi_e \tag{3}$$

$$W_a = \gamma_{LV}(1 + \cos\theta) \leqslant 2\gamma_{LV} \tag{4}$$

$$W_a = 2[\alpha_L\alpha_S + \beta_L\beta_S] \tag{5}$$

$$\frac{W_a}{2\alpha_L} = \alpha_S + \beta_S(\beta_L/\alpha_L) \tag{6}$$

TABLE II
Symbols and nomenclature

Liquid–solid interactions

γ_{LV} = liquid–vapor surface tension
γ_{SV} = solid–vapor surface tension
γ_S^o = surface tension of virgin solid surface in vacuum
π_e = surface energy reduction due to immersion in ambient vapor phase
α_L, β_L = square root of the respective (London) dispersion γ_{LV}^d and (Keesom) polar γ_{LV}^p parts of γ_{LV}
α_S, β_S = square roots of respective dispersion γ_{SV}^d and polar γ_{SV}^p parts of γ_{SV}
W_a = nominal work of adhesion
θ = liquid–solid contact angle

Modified Griffith fracture criteria

σ_c = critical crack propagation stress
γ_G = Griffith surface energy for fracture
E = Young's modulus
c = crack length
α_1, β_1 = matrix surface properties
α_2, β_2 = surface properties of environment
α_3, β_3 = fiber surface properties

Cumulative damage model

ϕ = fractional degree of degradation
W_λ = initial fracture energy
W_∞ = final fracture energy at t
W_t = fracture energy at time t
t = cumulative environmental esposure time
λ = time relating to initiation of degradation
b = a time exponent of the degradation process
K = a system constant
a_T, a_M, a_c = dimensionless time shift factors relating to thermal (T), mechanical (M), and environmental (c) stress effects.

The symbols of Eq. (1) through Eq. (6) are defined in Table II. When reference is made to the solid-vapor surface tension γ_{SV} of high energy solids such as glass, ceramics, metals, or metal oxides, a common confusion exists by assuming $\gamma_{SV} \simeq \gamma_{S^o}$ where γ_{S^o} is the surface tension (or surface free energy) of the virgin solid surface in vacuum. When such surfaces are exposed to ambient atmosphere, studies show that Π_e is very nearly equal to γ_{S^o} which points out that γ_{SV} is primarily influenced by the chemical constitution of the adsorption layer on the solid surface.[4,5] In contrast, organic or polymeric surfaces,

with low initial values for γ_{S^0}, generally display $\Pi_e \simeq 0$ so that $\gamma_{SV} \simeq \gamma_{S^0}$ and the determined value of γ_{SV}, measured under ambient atmospheric conditions, correlates closely with the virgin surface in vacuum.

The determination of γ_{SV} is, of course, relevant to interfacial adhesion studies since in polymer matrix composites the interfacial bond is normally formed or broken under ambient atmospheric conditions. Values of $\gamma_{LV}{}^d$ and $\gamma_{LV}{}^p$ may be experimentally determined by a combination of surface tension and interfacial tension measurements.[7,8] The problem remains to indirectly measure the values of $\gamma_{SV}{}^d = \alpha_S{}^2$, $\gamma_{SV}{}^p = \beta_S{}^2$ for the solid surface of interest. Experimental values of nominal work of adhesion W_a as defined by Eq. (4) for liquid–solid contact angle $\theta \geqslant 0$ may be analyzed in terms of either Eq. (5) or Eq. (6). From Eq. (6) we recognize a simple method of graphical analysis wherein a plot of $W_a/2\alpha_L$ versus β_L/α_L defines α_S as an intercept at $\beta_L/\alpha_L = 0$ and β_S as a slope.[5] A determinant method of simultaneous solutions of Eq. (5) has also been described which provides computed average values for $\gamma_{SV}{}^d$, $\gamma_{SV}{}^p$ and γ_{SV} in conjunction with the respective standard deviations $\pm\delta^d$, $\pm\delta^p$, and $\pm\delta$.[4] In fact, the graphical method via Eq. (6) and the computational method via Eq. (5) are complementary and will both be exploited in this discussion.

The recent extension of the adsorption theory of interfacial interactions provides a generalizing statement for the critical value of the Griffith fracture stress σ_c under normal plane stress loading by the following relations:[6]

$$\sigma_c = \left(\frac{2E\gamma_G}{\pi c}\right)^{1/2} = \left(\frac{2E}{\pi c}\right)^{1/2}(R^2 - R_0{}^2) \geqslant 0 \tag{7}$$

$$R_0{}^2 = \tfrac{1}{4}[(\alpha_1 - \alpha_3)^2 + (\beta_1 - \beta_3)^2] \tag{8}$$

$$R^2 = (\alpha_2 - H)^2 + (\beta_2 - K)^2 \tag{9}$$

$$H = \tfrac{1}{2}(\alpha_1 + \alpha_3) \tag{10}$$

$$K = \tfrac{1}{2}(\beta_1 + \beta_3) \tag{11}$$

The nomenclature of Table II defines the symbols which appear in Eq. (7) through Eq. (11). Several recent experimental studies have shown that the strength and fracture energy of adhesive joints can be systematically varied due to environmentally controlled failure.[9,10] The results of these studies have been successfully rationalized in terms of the modified Griffith model defined in Eq. (7) through Eq. (11).[6] One of the important results evident from current analysis of environmentally controlled failure in viscoelastic media relates to a clarification of the energy terms in the Orowan relation:[11]

$$\sigma_c = \left[\frac{2E}{\pi c}(\gamma_G + W_P)\right]^{1/2} \tag{12}$$

where γ_G is the reversible Griffith fracture energy and W_P is the dissipated plastic (or viscoelastic) work of fracture. Present analysis indicates that for the case where $W_P \gg \gamma_G$ these two energies are not independent additive terms to the total fracture energy $W = \gamma_G + W_P$. Under environmentally controlled failure a qualitative relation $\gamma_G^{1/2} \propto W_P$ has been shown which indicates that small variations in γ_G induced by environmental effects produce large variations in W_P.[6]

Cumulative damage of composite systems subjected to accelerated ageing under adverse environments has recently been treated by Halpin and co-workers.[12,13] A special statement of the Halpin-Polley relation[12] as applied to the time dependent changes of total work of fracture W_t at time t may be expressed as a dimensionless function of the degree of degradation ϕ as follows:

$$\phi = \frac{W_\lambda - W_t}{W^\lambda - W^\infty} = \exp\left[-K(t - \lambda)^b / a_T a_M a_c\right] \tag{13}$$

taking logarithms we obtain:

$$-\ln \phi = K(t - \lambda)^b / a_T a_M a_c \tag{14}$$

$$ln\,(-\ln \phi) = b \ln (t - \lambda) + \ln (K/a_T a_M a_c) \tag{15}$$

The parameters which define Eq. (13) through Eq. (15) are individually described in the nomenclature of Table II. Equation (15) defines a linear function of $\ln(-\ln \phi)$ versus $\ln(t - \lambda)$ with slope b for the case where $K/a_T a_M a_c =$ constant. The important feature of Eq. (13) is the possibility of evaluating the effects of cumulative damage in terms of a rate process at nominal times of environmental exposure and analyzing for a predicted fracture energy W_∞ at infinite time $t = \infty$ based upon linearization of data as described in Eq. (15).

The relations set forth in this section form the basis for the analysis of the mechanisms of interfacial bonding and environmental stability in a graphite fiber/epoxy matrix composite material. The analysis is specifically focused on the interfacial factors which produce moisture sensitivity in polymer matrix composites.

MATERIALS AND METHODS

Resin impregnated tapes of uncured Hercules 3002 epoxy resin with Hercules Type A untreated graphite fiber (procured from Ferro Corp.) and Hercules Type AS treated fiber (procured from Fiberite Corp.) were selected for this study. For wettability studies the uncured resin was dissolved away from the uniaxial fiber array using methyl ethyl ketone (MEK) solvent. The Type A and Type AS fibers used in wettability studies were further cleaned in absolute ethanol and distilled water. Films of the 3002 epoxy resin were cast on glass

plates from MEK solvent and vacuum dried for one week at 22°C prior to measurement of wettability studies in the uncured state. A portion of these films, cured under dry N_2 atmosphere for 100 min at 177°C, also underwent wettability studies.

Single fibers of graphite Type A (untreated) and Type AS (treated) fibers were analyzed for wettability using the micro Wilhelmy plate technique described by Neumann and Tanner and also Mozzo and Chabord.[14,15] In this measurement the contact force ΔM(gm) between a single fiber of circumference C and a liquid of surface tension γ_{LV} is described by the following relation:[14,15]

$$\Delta M = \frac{\gamma_{LV} C \cos\theta}{g} \tag{16}$$

where θ is the *advancing* liquid–solid contact angle and $g = 980.6$ dyn/gm. Wetting liquids which form zero contact angle on the fiber surface provide $\cos\theta = 1.0$ in Eq. (1) and permit direct calculation of fiber circumference. The force ΔM is measured by a recording CAHN electrobalance whose sensitivity is $\pm 0.05\ \mu$ gm.

Advancing liquid–solid contact angles θ for uncured and cured films of the epoxy matrix resin were determined at 20°C in the B-100 environmental chamber of the NRL goniometer (Rame-Hart Inc.) using the sessile drop method. The test liquids utilized in wettability studies for both fiber and resin components of this reinforced composite are listed in descending order of surface tension values in Table III. The surface tensions of the test liquids

TABLE III
Surface tension properties of test liquids at 20°C

Test liquid	γ_{LV} [	γ_{LV}^d dyn/cm	γ_{LV}^p]	$2a_L$ (dyn/cm)$^{1/2}$	$\beta_L a_L$
Water	72.8	21.8	51.0	9.34	1.53
Glycerol	64.0	34.0	30.0	11.66	0.94
Formamide	58.3	32.3	26.0	11.37	0.90
Diiodomethane	50.8	48.5	2.3	13.93	0.22
Ethylene glycol	48.3	29.3	19.0	10.83	0.81
1-Bromonapthalene	44.6	44.6	0.0	13.36	0.00
Glycol PG-E-1200	43.5	28.2	15.3	10.62	0.74
Tricresyl phosphate	40.9	39.2	1.7	12.52	0.21
Glycol PG-15-200	36.6	26.0	10.6	10.20	0.64
Glycol PG-P-1200	31.3	24.5	6.8	9.90	0.53
n-Hexadecane	27.6	27.6	0.0	10.51	0.00
n-Dodecane	25.4	25.4	0.0	10.08	0.00
Ethanol (abs.)	22.4	17.0	5.4	8.24	0.56

were determined by several techniques which include platinum-iridium Wilhelmy plate, glass capillary rise, or Du-Nouy ring method. Agreement between experimental and literature values of liquid surface tension, generally

within ± 0.5 dyn/cm, is taken as evidence of purity and literature values of $\gamma_{LV}{}^{d}$ and $\gamma_{LV}{}^{p}$ are applied in the surface energy analysis.

The curing reactions of the two resin impregnated tapes were evaluated by differing scanning calorimetry (DSC). The DSC experiment measures the net rate of heat input or output by the sample H/t as a function of time t or temperature T at constant thermal scan rate $K = 10°C/min$. A special analysis of two successive thermal scans of the same sample isolates the net rate of curing in terms of H_p/t and the apparent heat of curing ΔH_p. The detailed description of measurement and analysis using DSC is described by Kaelble and Cirlin[16] and is followed in the present experiments of this study.

The curing procedure for preparation of thick laminate sections of unidirectional reinforced graphite AS fiber/3002 epoxy matrix includes the following steps. After lay up and bagging the laminate is held under vacuum for 30 minutes at 22°C prior to installation in the autoclave. The laminate is heated to 121°C in 30 min under vacuum. After 30 minutes at 121°C the autoclave pressure is raised to 100 psi over a period of 10 minutes and the 121°C temperature maintained for a total time of one hour. The autoclave temperature is then raised to 177°C and maintained for 2 hrs at 177°C and 100 psi pressure to complete cure. The laminate is then cooled to 66°C under 100 psi autoclave pressure. The laminate is removed from the autoclave, debagged, and postcured for 2 hrs at 177°C in a circulating air oven.

Preliminary tests of the cured laminates showed that the volume fraction of fiber reinforcement was 0.60 ± 0.02. Mechanical property measurements at ambient temperature indicated a longitudinal flexure strength of $18{,}150 \pm 680$ kg/cm^2, a short beam shear strength of 1160 ± 84 kg/cm^2, and average transverse tensile strength of 344 kg/cm^2. Samples of the cured uniaxially reinforced laminate of Type AS graphite fiber/3002 epoxy matrix composite were cut by liquid cooled diamond saw to sample length of 3.00 cm and square cross section of 0.50 cm. Following the design of Tatersall and Tappin,[17,18] the samples were center grooved with a 0.05 cm diamond saw to form a cross section in the form of an isoceles triangle. Uniaxial fiber reinforcement is parallel to sample length in all samples. These samples were aged for varied times under 100 percent R.H. and water immersion conditions at 100°C using a reflux of distilled water. Samples withdrawn from the aging environment were promptly tested for fracture toughness in three point bending using a crosshead rate of 0.5 cm/min and test temperature of 22°C. The geometry of flexure loading initiates a crack at the apex of isosceles triangle section which then propagates downward to the base of the triangle. The force-displacement integral directly recorded by the integrator accessory of the Instron testing machine is taken as a direct measure of fracture energy W_b and is further analyzed. Sample weighing immediately after removal from

the high moisture environment and subsequent to extended dessication over anhydrous calcuim sulphate permits determination of moisture content at the time of fracture energy testing.

RESULTS AND DISCUSSION

This section is subdivided into several parts which individually examine and discuss the separate phases of the experimental study.

a Interfacial bonding

The design of the wettability experiment is based upon the application of heterogeneous test liquids whose γ_{LV}^{p} values do not vary systematically with liquid surface tension γ_{LV}. Inspection of Table III shows that β_L/α_L does not vary in a systematic fashion with γ_{LV}. The liquids should range from completely nonpolar (saturated hydrocarbons) to highly polar (formamide, glycerol, water) in surface tension properties.

The measured values of wetting force ΔM between test liquid and Type A and Type AS graphite fibers are presented in Table IV and Table V, respectively. Microscopic examination of these fibers revealed a smooth surface and essentially circular cross section typical of polyacrylonitrile (PAN) precursor material. The remaining columns of Table IV and Table V tabulate the data conversions based upon appropriate application of Eq. (16) and Eq. (4) through Eq. (6).

TABLE IV

Micro Wilhelmy plate measurement of wettability for Type A graphite fiber at 23°C

γ_{LV} (dyn/cm)	ΔM (μ gm)	cos θ	W_a dyn/cm	$W_a/2\alpha_L$ (dyn/cm)$^{1/2}$	β_L/α_L
72.8	181	0.8299	133.22	14.26	1.53
64.0	182	0.9492	124.75	10.70	0.94
58.3	131	0.7500	102.03	8.97	0.90
50.8	115	0.7556	89.18	6.40	0.22
48.3	137	0.9467	94.03	8.68	0.81
44.6	126	0.9430	86.66	6.49	0.00
43.5	130[a]	1.000	—	—	0.74
36.6	106	0.9667	71.98	7.06	0.64
31.3	94[a]	1.000	—	—	0.53
25.4	71	0.9330	49.10	4.87	0.00

[a] Wetting condition with cos $\theta = 1.0$. Calculated fiber circumference $C = g\Delta M/\gamma_{LV} = 29.38 \pm 0.08$ μm.

The plots of Wilhelmy plate force ΔM for the advancing contact angle condition versus liquid surface tension γ_{LV} are shown for Type A fiber in Figure 1 and Type AS fiber in Figure 2. The slope of the linear curves of Figure 1 and Figure 2 define the fiber circumference C and maximum wetting

TABLE V

Micro Wilhelmy plate measurement of wettability for Type AS graphite fiber at 23°C

γ_{LV} (dyn/cm)	ΔM (μ gm)	cos θ	W_a (dyn/cm)	$W_a/2\alpha_L$ (dyn/cm)$^{1/2}$	β_L/α_L
72.8	172	0.8966	138.07	14.68	1.53
64.0	161	0.9547	125.10	10.73	0.94
58.3	120	0.7811	103.84	9.13	0.90
50.8	102	0.7620	89.51	6.43	0.22
48.3	120	0.9429	93.84	8.66	0.81
44.6	111	0.9445	86.72	6.49	0.00
43.5	114[a]	1.00	—	—	0.74
36.6	94	0.9747	72.27	7.09	0.64
31.3	83[a]	1.00	—	—	.53
25.4	63	0.9413	49.31	4.89	0.00
22.4	56.3	0.9413	43.49	5.28	0.53

[a] Wetting condition with cos θ = 1.0. Calculated fiber circumference $C = g\Delta M/\gamma_{LV}$ = 25.86 $\pm$ 0.15 μ m.

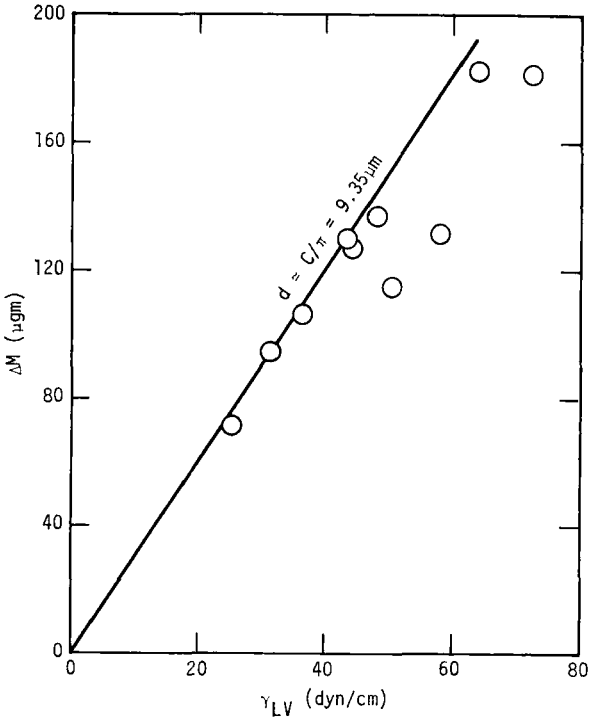

FIGURE 1 Wilhelmy plate force ΔM versus liquid surface tension γ_{LV} for graphite Type A fiber.

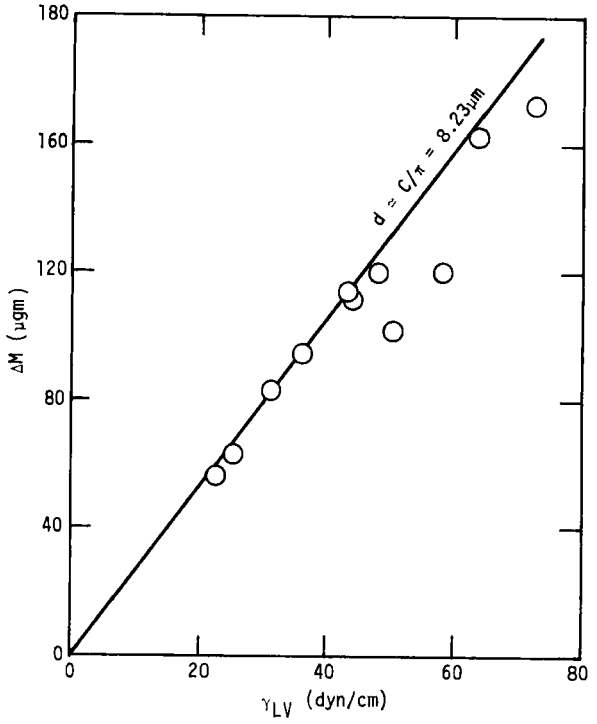

FIGURE 2 Wilhelmy plate force ΔM versus liquid surface tension γ_{LV} for graphite Type AS fiber.

force ΔM_{max} for $\cos\theta = 1.00$. The apparent diameters $d \simeq C/\pi$ correlate closely with values determined by microscopic examination of the fibers. Liquids which display finite contact angle $\theta \geqslant 0$ provide data points below the ΔM_{max} curve.

The upper portion of Figure 3 presents the wetting data for Type A fiber in the format suggested by Zisman and coworkers[19] where a linear plot of $\cos\theta$ versus γ_{LV} extrapolated to the condition for wetting $\cos = 1.0$ defines the critical surface tension γ_c for the solid surface. This upper Figure 3 shows an extreme data scatter which is very characteristic of this series of test liquids when interacting with polar solid surfaces. In other words, it is evident that a single parameter description of solid surface tension, as defined by γ_c, is insufficient in predicting a criteria for wetting and non-wetting.

The lower portion of Figure 3 presents these same data in the format defined by Eq. (5). The solid curve is obtained from computed average values of γ_{SV}^d and γ_{SV}^p using the determinant method, while the dashed curves describe uncertainty in γ_{SV}^d and γ_{SV}^p described by the standard deviations $\pm\delta^d$ and $\pm\delta^p$. It is evident that Eq. (5) or Eq. (6) characterizes the liquid–solid

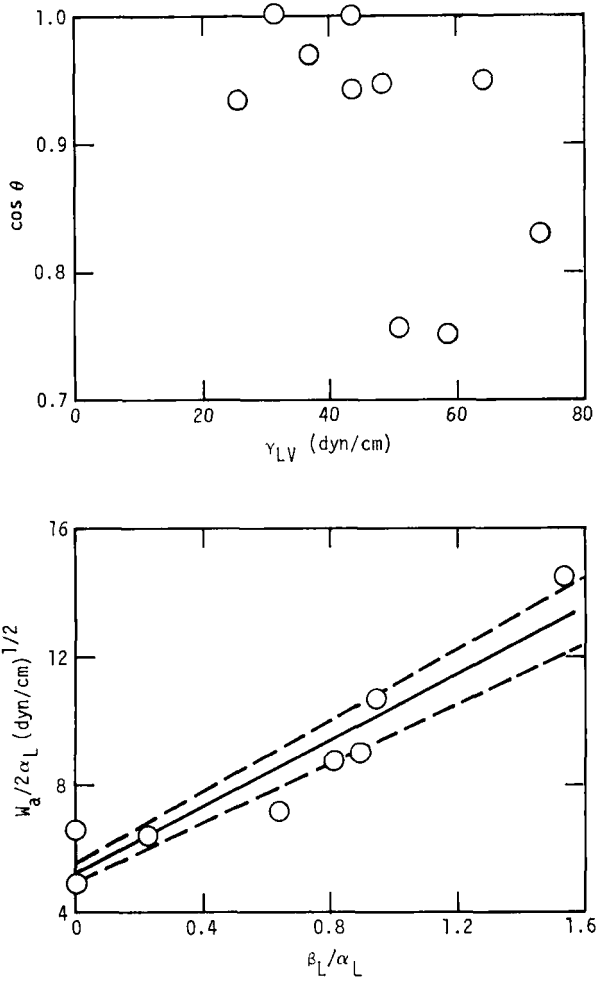

FIGURE 3 Variation of cos θ versus γ_{LV} (upper view) and $W_a/2\alpha_L$ versus β_L/α_L (lower view) for graphite Type A fiber.

interactions for Type A graphite with greater precision than the usual plot of cos θ versus γ_{LV}. Most importantly the wetting properties of water with $\beta_L/\alpha_L = 1.53$ are correlated on a single function with those of nonpolar dodecane with $\beta_L/\alpha_L = 0$.

The upper and lower portions of Figure 4 present an equivalent data display for the wetting properties of the test liquids on graphite Type AS fiber. The high slope of the $W_a/2\alpha_L$ versus β_L/α_L curves presented by the determinant analysis show that both Type A and Type AS fibers display strong polar interactions with the polar test liquids.

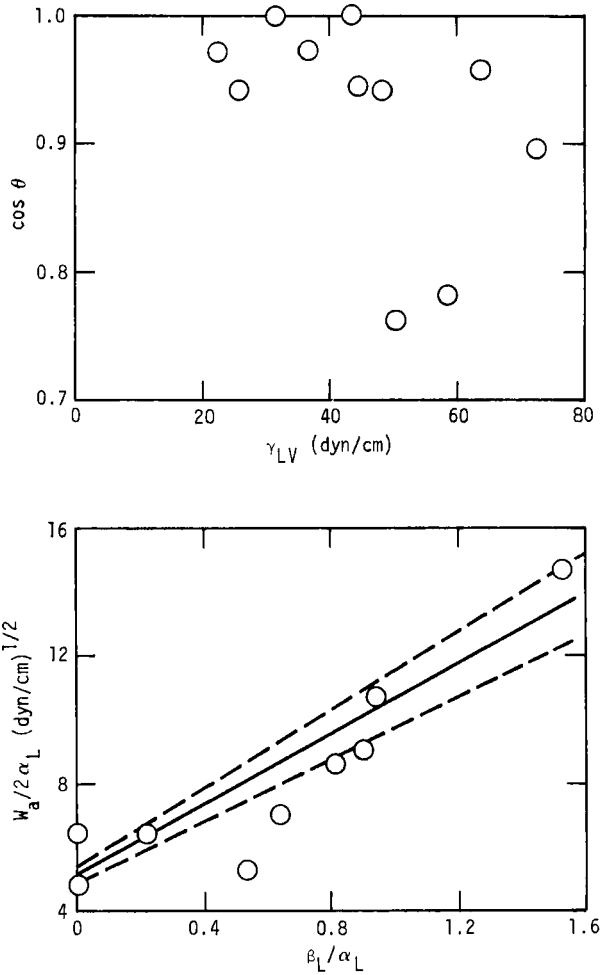

FIGURE 4 Variation of cos θ versus γ_{LV} (upper view) and $W_a/2a_L$ versus β_L/a_L (lower view) for graphite Type AS fiber.

The values of cos θ and $W_a/2\alpha_L$ determined from advancing contact angle measurement of sessile drops on films of uncured and cured epoxy resin 3002 are summarized in Table VI. The data displays of Figure 5 show considerable scatter of cos θ versus γ_{LV} (upper view) and reasonable resolution on a $W_a/2\alpha_L$ versus β_L/α_L function (lower view) for the uncured epoxy resin. A similar presentation in Figure 6 for the wettability of the cured resin film of epoxy 3002 displays a result similar to Figure 5 for the uncured material. The solid and dashed curves of Figure 5 (lower view) and Figure 6 (lower view)

TABLE VI
Wettability data for uncured and cured epoxy resin 3002 at 20°C

	3002 Resin		Uncured		Cured	
γ_{LV} (dyn/cm)	$2a_L$ (dyn/cm)$^{1/2}$	β_L/a_L	cos θ	$W_a/2a_L$ (dyn/cm)$^{1/2}$	cos θ	$W_a/2a_L$ (dyn/cm)$^{1/2}$
72.8	9.34	1.53	0.8434	14.37	0.7965	14.00
64.0	11.66	0.94	0.7891	9.82	0.7570	9.64
58.3	11.37	0.90	0.9664	10.08	0.9348	9.92
50.8	13.93	0.22	0.8712	6.82	0.8070	6.59
48.3	10.83	0.81	0.8830	8.40	0.9617	8.75
44.6	13.36	0.00	0.9252	6.43	0.8678	6.24
43.5	10.62	0.74	0.9285	7.90	0.9699	8.07
31.3	9.90	0.53	0.9816	6.26		

present the computed values of $\gamma_{SV}{}^d \pm \delta^d$ and $\gamma_{SV}{}^p \pm \delta^p$ in the format described by Eq. (6).

The results of the determinant calculations for solid–liquid interactions presented graphically in Figure 3 through Figure 6 are summarized in Table VII. This analysis shows that Type A and Type AS graphite fibers are quite similar with respect to both $\gamma_{SV}{}^d$ and $\gamma_{SV}{}^p$. It is also evident that both fiber surfaces display a strong polar $\gamma_{SV}{}^p$ contribution to the total surface tension $\gamma_{SV} = \gamma_{SV}{}^d + \gamma_{SV}{}^p$. The low magnitude of $\gamma_{SV} = 55 \pm 2$ dyn/cm and the polar/nonpolar ratio $\beta_S/\alpha_S \simeq 0.97 \pm 0.05$ for fiber Type A and Type AS explain why most organic liquids fail to wet this type of solid surface.

The surface properties of the matrix resin show statistically significant reductions in both $\gamma_{SV}{}^p$ and γ_{SV} as a result of curing. It may be noted that the surface properties of the cured 3002 epoxy resin very closely resembles the fiber surface properties. At first glance this would appear to indicate that the solvent removal of resin from fiber was incomplete and the fiber surface was contaminated by a multimolecular layer of resin. Comparative data for other graphite fiber surfaces, where the fiber surface is not exposed to prior resin contact, are summarized in the upper portion of Table VIII and show close correlation with the values of $\gamma_{SV}{}^d$ and $\gamma_{SV}{}^p$ shown by this study for Type A and Type AS fiber.

The lower portion of Table VIII presents solid surface tension properties for three chemical classes of matrix resins determined in previous studies. Comparison of these data with the resin surface energy values reported in Table VII shows that both uncured and cured forms of 3002 epoxy resin display extraordinarily high values of both $\gamma_{SV}{}^p$ and γ_{SV}.

b) Chemo-rheology of curing

The conversion of the uncured matrix from its initial bonding state to its final holding state as a fully cured material can be readily monitored by DSC

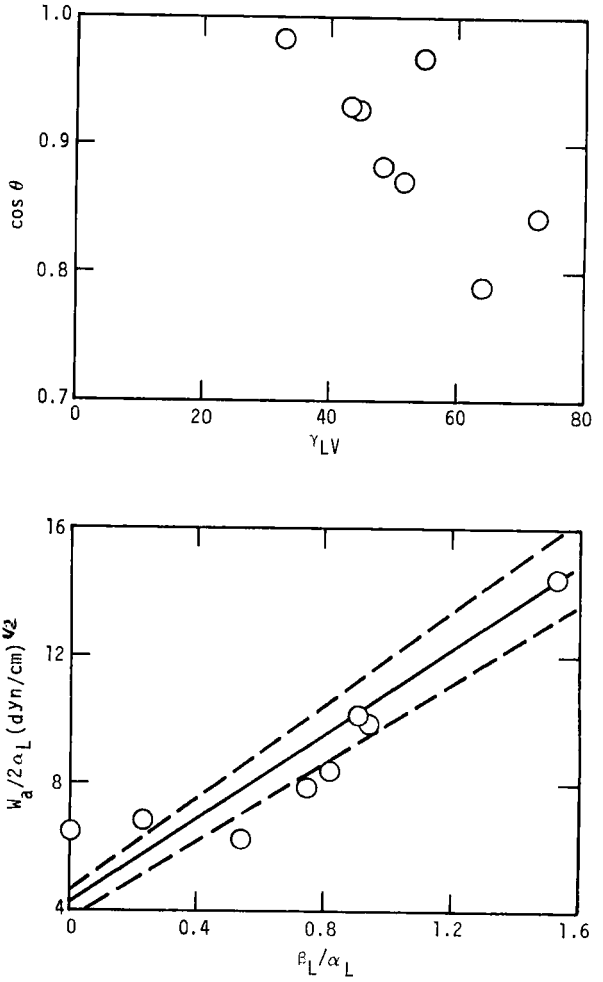

FIGURE 5 Variation of cos θ versus γ_{LV} (upper view) and $W_a/2\alpha_L$ versus β_L/α_L (lower view) for uncured 3002 epoxy resin.

characterization. Table IX summarizes typical results of DSC scans for uncured composites of Type A fiber and Type AS fiber in 3002 epoxy resin. Experimental curves of the exothermic rate of heat release H_p/t due to curing for the experiments described by Table IX are shown in Figure 7. The reaction kinetics as defined by the temperature of maximum reaction rate T^* and the apparent heat of curing ΔH_p obtained by integrating the area beneath the H_p/t versus t curve are comparable for the two fiber/matrix systems. This result confirms that the differing surface treatments that characterize Type A

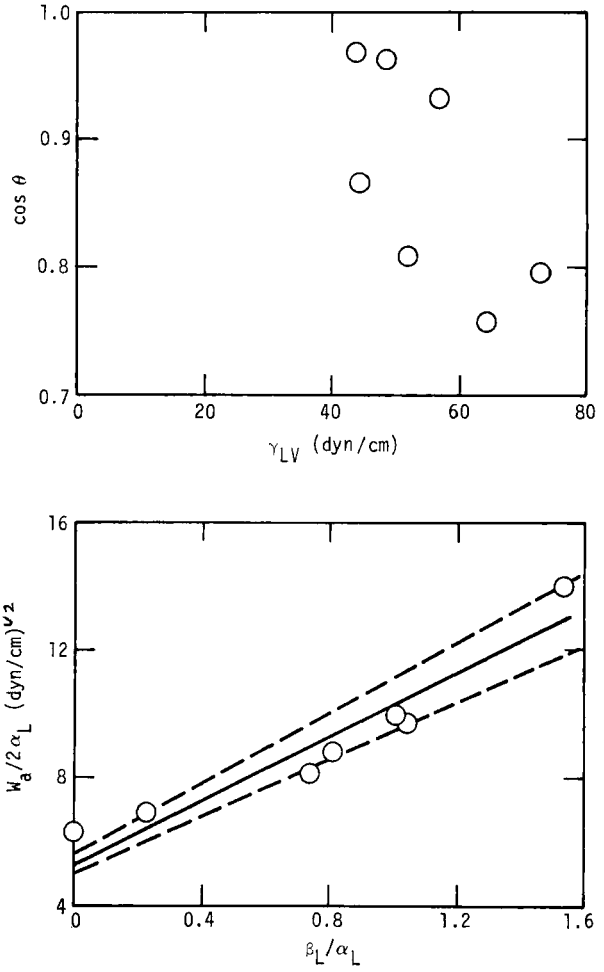

FIGURE 6 Variation in cos θ versus γ_{LV} (upper view) and $W_a/2\alpha_L$ versus β_L/α_L (lower view) for cured 3002 epoxy resin.

and Type AS fibers do not produce substantially different curing kinetics or extents of reaction in the 3002 epoxy resin.

c) Environmental effects on fracture energy

The primary result of the surface energy analysis and chemo-rheology studies already discussed has indicated that Type A and Type AS graphite fibers display essentially equivalent physical and chemical interactions with the 3002 epoxy matrix material. At this point in the study efforts were concentrated on

TABLE VII

Summary of surface energy analysis by the determinant method for graphite fibers and resin matrix materials (for method see ref.)

	$\gamma_{sv}^d \pm \delta^d$ (dyn/cm)	$\gamma_{sv}^p \pm \delta^p$ (dyn/cm)	$\gamma_{sv} \pm \delta$ (dyn/cm)
Fiber			
Type A (untreated)	27.9 ± 2.9	26.4 ± 4.7	54.3 ± 2.5
Type AS (treated)	26.7 ± 3.0	29.9 ± 5.8	56.6 ± 3.5
Matrix			
uncured 3002 Epoxy	27.9 ± 4.0	32.2 ± 6.9	60.1 ± 3.4
cured 3002 Epoxy	28.9 ± 3.2	25.0 ± 4.7	53.9 ± 2.0

TABLE VIII

Summary of surface tension properties for reinforcing fibers and matrix resins calculated by the determinant method (ref. 5).

	$\gamma_{sv}^d \pm \delta^d$ (dyn/cm)	$\gamma_{sv}^p \pm \delta^p$ (dyn/cm)	$\gamma_{sv} \pm \delta$ (dyn/cm)
Graphite Fiber			
Hercules HT-S®	25.9 ± 1.5	25.7 ± 3.3	51.6 ± 2.3
Hercules HM-S®	26.1 ± 2.1	26.8 ± 4.1	52.8 ± 2.7
Morganite II®	27.4 ± 1.6	27.3 ± 4.1	54.7 ± 3.1
Modmor II® (Whittaker)	28.3 ± 3.5	29.4 ± 6.0	58.2 ± 2.8
Polysulfone Resins			
Polysulfone P-1700® (Union Carbide)	26.1 ± 2.0	3.6 ± 1.6	29.7 ± 2.7
Astral 380® (3M Co.)	32.6 ± 3.1	16.1 ± 4.3	48.6 ± 3.2
Astral 360® (3M Co.)	25.4 ± 2.1	19.2 ± 4.5	44.6 ± 3.4
Polyimide Resins			
Skybond-708® (Monsanto)	34.5 ± 3.4	11.7 ± 4.8	46.2 ± 1.9
Skybond-709® (Monsanto)	36.0 ± 3.5	10.1 ± 3.7	46.1 ± 3.0
XPI-182® (Monsanto)	36.7 ± 3.1	8.4 ± 1.9	45.2 ± 1.6
Epoxy-Phenolic Resin			
H.T. 424® (Amer. Cyan.)	30.3 ± 4.5	12.0 ± 2.6	42.3 ± 2.3

® = Trademark

the Type AS fiber/3002 epoxy matrix systems in terms of analyzing environmental effects upon fracture energy.

Introducing the results of the surface energy analysis into Eq. (7) through Eq. (11) permits an analysis of immersion environment (phase 2) effects upon the critical fracture stress described in the modified Griffith model. The interface between cured 3002 epoxy (phase 1) and Type AS fiber is described

TABLE IX

Summary of DSC analysis of curing

Prepreg system	(1) Graphite Type A/ 3002 epoxy resin	(2) Graphite Type AS/ 3002 epoxy resin
Sample wt (mgm)	5.25	6.35
Min. Scan Temp.-T_1 (°K)	300	300
Max. Scan Temp.-T_2 (°K)	510	510
Scan Rate-K (°K/min)	10	10
Hold Time at T_2 to complete cure (min)	100	100
Temp of Max-H/t (°K)	468	455
Apparent Heat of Cure ΔH_p (cal/gm)	40.9	35.1

by the average $\gamma_{SV}{}^d$ and $\gamma_{SV}{}^p$ properties of these solid phases (see Table VII). For the resin we obtain values $\alpha_1 = 5.38\ (\text{dyn/cm})^{1/2}$ and $\beta_1 = 5.0\ \text{dyn/cm})^{1/2}$. For the type AS fiber the parameters $\alpha_3 = 5.17\ (\text{dyn/cm})^{1/2}$ and $\beta_3 = 5.45\ (\text{dyn/cm})^{1/2}$ define the respective dispersion and polar surface properties. These matrix and fiber surface properties are represented on the diagram of α

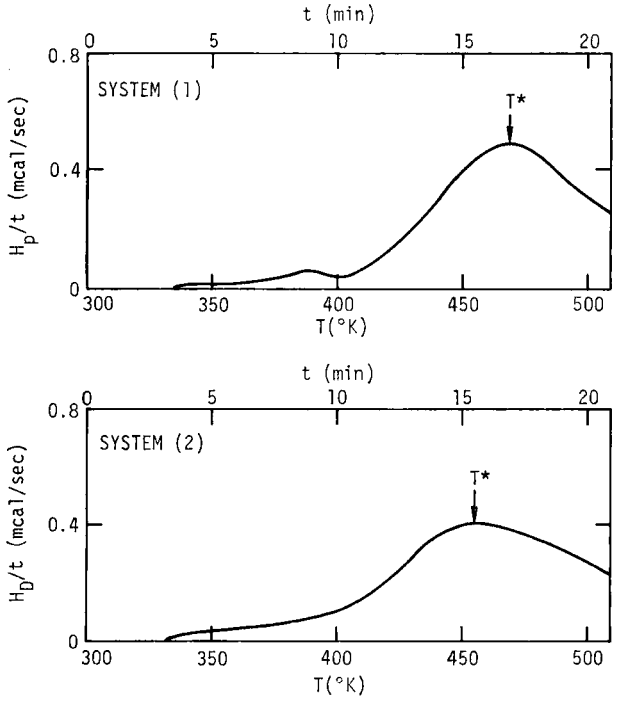

FIGURE 7 DSC curves of H_p/t versus temperature T or time t for curing of Type A graphite/3002 epoxy matrix (upper curve) and Type AS/3002 epoxy matrix (lower curve).

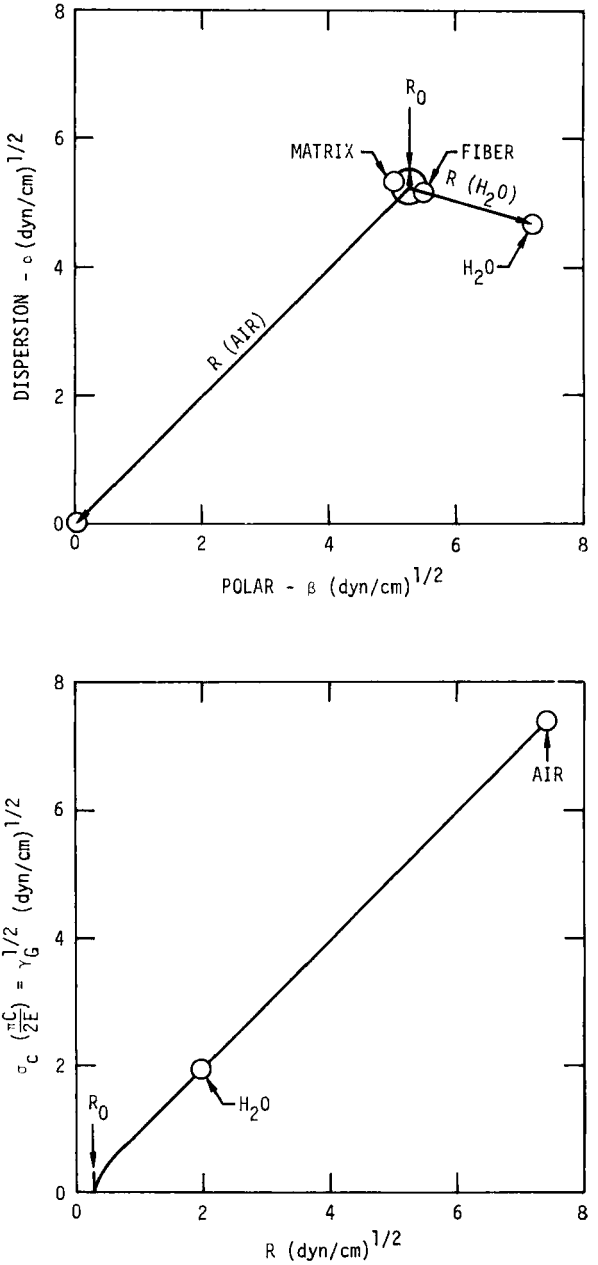

FIGURE 8 (Upper) Matrix (Phase 1) and Fiber (Phase 3) surface properties relative to immersion phases of air and water (Phase 2) (Lower) Griffith failure criteria σ_c ($\pi c/2E$) = $\gamma_G^{1/2}$ for resin/fiber interface in air (R = 7.46) and water (R = 1.96).

versus β shown in the top view of Figure 8. Application of Eq. (8) shows that a small radius $R_0 = 0.25$ (dyn/cm)$^{1/2}$, indicated in the top view of Figure VIII, defines the region of α_2 versus β_2 where the critical fracture stress $\sigma_c = 0$. The relative magnitudes of the critical fracture stress in air and water immersion are represented by R(air) and $R(H_2O)$ in the top view of Figure 8. The bottom view of Figure 8 graphs the function of $\sigma_c(\pi C/2E)$ versus the parameter R of Eq. (7) to show a master function which includes air and water immersion environments as two special cases.

The prediction from the analysis for critical fracture stress is that the fiber/matrix bond should be substantially stronger in air than in water. The top view of Figure 8 shows that the surface properties of both matrix and fiber lie much closer to those of water, with $\alpha_2 = 4.67$ dyn/cm and $\beta_2 = 7.46$ dyn/cm, than those of air with $\alpha_2 = \beta_2 = 0$. The energy required to create a fracture surface at the bonded interface is $\gamma_G = (R^2 - R_0^2)$. Reducing the value of R by water immersion, is shown by Figure 8 to correlate with the polar character of both the matrix and fiber surface properties which results in a water susceptible interface.

The results of the experimental study on the effects of moisture exposure upon the fracture energy in Type AS fiber/3002 matrix composite material are summarized in Table X. This experiment was designed to utilize the cumulative damage logic as described in Eq. (13) through Eq. (15). As may be noted in Table X, both 100 percent R.H. exposure and water immersion at 100°C produce rapid degradation of fracture energy from initial values of $W = 51.3 \pm 2.5$ kg/cm at zero exposure time about $W \leqslant 30 \pm 2.0$ kg/cm at exposure times $t \geqslant 24$ hrs. The average values of the fracture work per unit of the triangular fracture area (units kg/cm = kg cm/cm^2) were analyzed in terms of the time function predicted by Eq. (15). The extreme high and low average values for fracture work in Table X were employed to describe $W_\lambda = 58.0$ kg/cm and $W_\infty = 28.0$ kg/cm. Selection of an initiation time $\lambda = 0$ for the cumulative damage process due to water immersion provides the calculated values of $\ln(-\ln \phi)$ and $\ln(t - \lambda)$ summarized in Table XI. The upper view of Figure 9 shows the data of Table XI plotted as a function of $y = \ln(-\ln \phi)$ versus $x = \ln(t - \lambda) = \ln t$. Both the water vapor and water immersion data points are fit reasonably well by a linear function:

$$y_c = 1.190 - 0.977\,X \tag{17}$$

obtained by linear least squares analysis of all data points. The standard deviation of experimental data defines a $\delta_y = \pm 0.496$ about y_c.

In Figure 9 the solid curve represents Eq. (17) and the dashed curves represent the uncertainties due to $\delta_y = \pm 0.496$. These dashed curves enclose the majority of data points and provide reasonable estimates for the time

TABLE X

Effects of moisture exposure on fracture energy (test condition = ambient atmosphere at 23°C and crosshead speed 0.05 cm/min)

Exposure condition	100 percent RH at 100°C			Water immersion at 100°C		
Exposure time (t) (hr)	Moisture content (% bw)	W_t (Kg/cm)	ave. W_t (Kg/cm)	Moisture content (% bw)	W_t (kg/cm)	ave. W_t (kg/cm)
0	—	48.8	51.3 ± 2.5	—	48.8	51.3 ± 2.5
	—	53.8		—	53.8	
2	0.27	52.8	49.1 ± 3.7	—	52.8	52.8
	0.58	45.4		0.34	—	
3	—	42.7	44.4 ± 1.7	0.37	54.1	53.4 ± 0.7
	0.17	46.0		0.33	52.7	
6	0.16	52.0	51.1 ± 1.0	0.40	66.6	58.0 ± 8.6
	0.20	50.1		0.40	49.4	
9	0.20	34.4	34.6 ± 0.2	0.26	34.1	34.4 ± 0.3
	0.21	34.8		0.25	34.6	
11	0.12	34'6	31.8 ± 2.8	0.27	37.0	36.1 ± 0.9
	0.11	29.0		0.27	35.2	
16	—	37.8	37.8	—	37.6	37.6
	—	—		—	—	
24	—	36.1	31.8 ± 4.3	0.49	29.8	28.2 ± 1.6
	0.50	27.5		0.48	26.6	
48	—	32.6	29.5 ± 3.2	—	24.1	28.0 ± 3.9
	0.25	26.3		0.31	31.8	
72	0.42	28.6	30.0 ± 1.4	3.20	32.6	29.3 ± 3.4
	0.35	31.4		0.76	25.9	

TABLE XI

Calculated values of degree of degradation ϕ based upon extreme values of fracture energy $W_\lambda = 58.0$ kg/cm and time for initiation of degradation $\lambda = 0$ hr.

Exposure		Water vapor			Water immersion		
t (hr)	$\ln(t - \lambda)$	W_t (kg/cm)	ϕ	$\ln(-\ln\phi)$	W_t (kg/cm)	ϕ	$\ln(-\ln\phi)$
2	0.693	49.1	0.297	0.194	52.8	0.173	0.562
3	1.10	44.1	0.453	−0.233	53.4	0.153	0.630
6	1.79	51.1	0.230	0.385	58.0	0.0	—
9	2.20	34.6	0.780	−1.392	34.4	0.787	−1.429
11	2.40	31.8	0.873	−1.996	36.1	0.730	−1.156
16	2.77	37.8	0.670	−0.915	37.6	0.680	−0.953
24	3.18	31.8	0.873	−1.996	28.2	0.993	—
48	3.87	29.5	0.950	−2.970	28.0	1.00	—
72	4.28	30.0	0.933	−2.669	29.3	0.957	−3.125

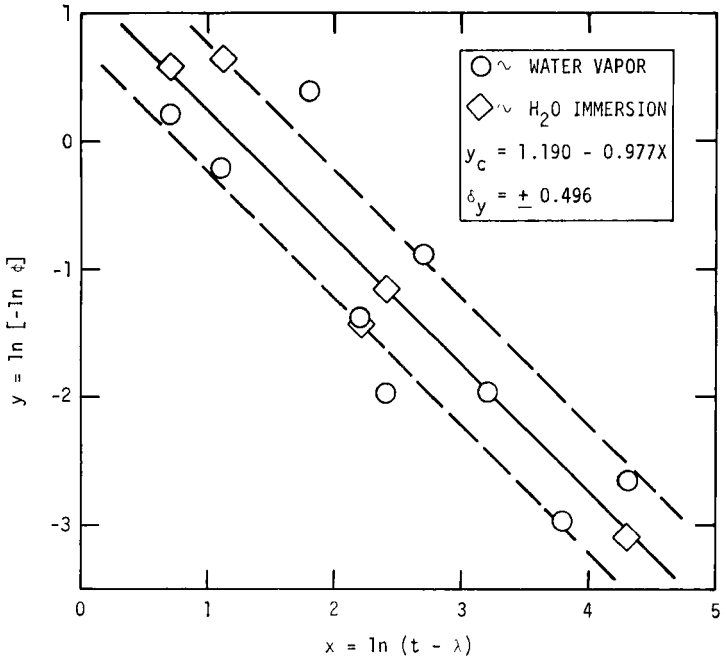

FIGURE 9 Analysis of the fractional degree of degradation ϕ in fracture energy W, versus degradation time $(t-\lambda)$ under high moisture environment at 100°C.

dependent variation of $y = \ln(-\ln \phi)$. The linearization of data on a plot of $\ln(-\ln \phi)$ versus $\ln t$ depends critically upon the proper selection of W_λ and W_∞. Linearization of $\ln(-\ln \phi)$ versus $\ln(t - \lambda)$ in conjunction with a minimization in the standard deviation δ_y provide implicit criteria for iterative procedures which optimize selected values of W_λ and W_∞. The analysis also indicates that exposure to 100 percent R.H. water vapor and water immersion at 100°C produce equivalent time dependent degradation in the fracture energy W_t of Type AS fiber/3002 epoxy composite material.

The results of the analysis shown on the logarithmic coordinates of Figure 9 are converted to more familiar format of fracture energy W_t versus environmental exposure time t in Figure 10. The geometry of the test specimen is illustrated in the lower portion of Figure 10. The predicted values of $W_\lambda = W_b(t = 0)$ and the extrapolated value of $W_\infty = W_b(t = \infty)$ are indicated on the left hand ordinate. The data points of Figure 10 represent the measured average values for W_t summarized in Table X. It is evident in Figure 10 that the total change in W_t with exposure time t is significant compared to the data scatter, as described by the dashed standard deviation curves.

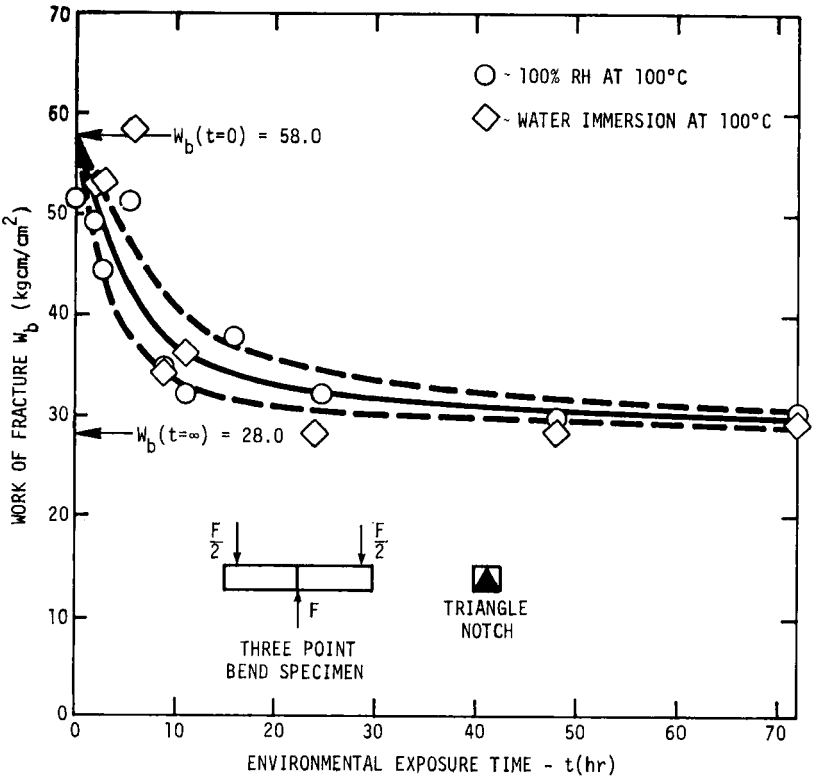

FIGURE 10 Measured loss in fracture energy W_b of reinforced composite under accelerated moisture aging [Fiber = Hercules Type AS graphite; Matrix = Hercules 3002 epoxy].

Special tests for moisture effects are reported in Table XII. These tests follow the same methods discussed in the data summary of Table X. Samples subject to no prior history of high moisture but broken under water immersion show essentially no decrease in fracture energy when compared to fracture in air. Tests involving cumulative damage by 100 percent R.H. or water immersion followed by desiccation at 23°C show that prior moisture damage produces an irreversible decrease in fracture energy. These latter results appear to confirm the lack of correlation between moisture content and fracture energy in the data of Table X.

The theoretical models for fracture energy in uniaxially reinforced composites describe a major contribution from the interfacial debonding and fiber pull out mechanisms.[18,20,21] The experimental data of Table X and

TABLE XII

Special tests for moisture effects

Exposure condition: Ambient atmosphere at 23°C
Test condition: Under water immersion at 23°C

Sample	Moisture Content (%)	W (kg/cm)	W_b (ave.) (kg/cm)
1	—	46.7	49.2 ± 2.50
2	—	51.7	

Exposure Condition: 100% RH at 100°C followed by desiccation at 23°C
Test Condition: Ambient atmosphere at 23°C

Exposure Time (t) (hr.)	Moisture Content (%)	W_b (kg/cm)	W_b (ave.) (kg/cm)
16	0	34.5	38.5 ± 4.0
16	0	42.5	

Exposure Condition: Water immersion at 100°C followed by desiccation at 23°C
Test Condition: Ambient atmosphere at 23°C

Exposure Time (t) (hr.)	Moisture Content (%)	W_b (kg/cm)	W_b (ave.) (kg/cm)
16	0	29.6	33.4 ± 3.8
24	0	37.2	

Table XII show that a time dependent process of progressive environmental damage of the interior interfaces of the composite produces a progressive decrease in fracture energy W. The negligible effect of testing under water immersion shown in Table XII tends to confirm that the major contribution to fracture energy is not influenced by the ambient test environment at the crack tip. Since interface debonding and fiber pull out mechanisms are essentially processes of bulk (or volumetric) failure which occur near, but not at the crack tip. it follows that W is dominated by the prior history of aging rather than the current environment at the instant of fracture. Conversely if the crack propagates in a simple crack opening mode without volumetric failure, the current environment at the crack tip at the instant of fracture should provide a dominating effect.[6]

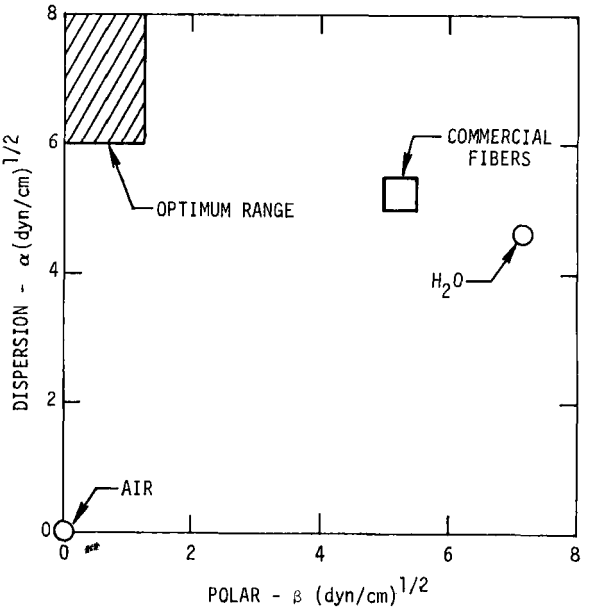

FIGURE 11 Shaded area of $\alpha \geq 6.0$, $\beta \leq 1.0$ (dyn/cm)$^{1/2}$ for optimized surface properties compared to surface properties of present commercial fibers and air and water immersion phases.

SUMMARY AND CONCLUSIONS

This study applies an extended form of the adsorption-interdiffusion (A-1) model for interfacial bonding to analyze and predict the water sensitivity of the fiber/matrix interface based upon thermodynamic arguments. Evaluation of the fracture energy for crack propagation perpendicular to the fiber axis shows a marked degradation in mechanical response due to cumulative damage by high moisture exposure. A specialized form of the Halpin-Polley cumulative damage model is succesfully applied to analyze the kinetics of degradation in fracture energy under exposure to high moisture environment and to predict long term response based upon short time testing.

The surface energy analysis of fiber and matrix components of graphite type AS/3002 epoxy matrix composite reveals a strong polar character for the fiber/matrix interfacial bond. Application of the Griffith fracture criteria for three phase interactions indicates that a water immersion environment will substantially decrease the critical stress σ_c for crack propagation under water immersion. Assuming the Griffith terms $(\pi c/2E)$ = constant (see Eq. (7)) independent of environment, the analysis predicts $\sigma_c(H_2O)/\sigma_c(\text{air}) \simeq 0.25$ for interfacial failure of graphite Type AS fiber/3002 epoxy matrix The substantial reduction of mechanical fracture energy under high humidity or

water immersion at 100°C shown in Figure 10 would appear to correlate with degradation of interfacial contributions to total fracture energy.

The present analysis would suggest that moisture insensitive interfaces in composite materials should be essentially nonpolar in character where $\beta_S \leqslant 1.0$ for both the matrix (phase 1) and fiber (phase 3). This low polar character would need to be complemented by an increased dispersion contribution $\alpha_S \geqslant 6.0\,(\text{dyn/cm})^{1/2}$ to provide Griffith fracture energy:

$$\gamma_G(\text{air}) \simeq \gamma_G(H_2O) = (R^2 - R_0^2) \geqslant 36\ \text{dyn/cm}$$

The optimized range of α_S and β_S described by this interfacial criteria is illustrated in the shaded region of the α versus β diagram of Figure 11. Also included in Figure 11 are the surface properties of present graphite and boron fibers, and the surface properties of potential immersion phases representing air and water. A final important criteria involves the necessity for the matrix phase to spontaneously wet and form a zero contact angle on the fiber during the process of impregnation so as to eliminate interfacial cavities and microvoids.[22,23]

Acknowledgments

The authors wish to acknowledge the kind cooperation of Dr. L. Lackman, Los Angeles Division, North American Rockwell Corporation, who furnished materials for study, and Dr. T. Smith, Science Center, for helpful discussions. This work was supported in part by the North American Rockwell IR and D Interdivisional Technology Program under the sponsorship of the Composite Technical Panel.

References

1. M. J. Salkind, "Interfaces in Composites," ASTM Spec. Tech. Pub. No. 452 (1969), p. 1.
2. S. Sterman, *J. Adhesion* **2**, 130 (1970).
3. D. A. Scola, and S. C. Brooks, *ibid.* 213 (1970).
4. D. H. Kaelble, *Physical Chemistry of Adhesion* (Wiley-Interscience, New York, 1971),
5. D. H. Kaelble, Proc. 23rd Int. Cong. of Pure Applied Chem., *8*, 265, Butterworths. London (1971).
6. D. H. Kaeble, "A Relationship Between the Adsorption-Interdiffusion (A-I) and the Griffith-Irwin (G-I) Failure Criteria," to be published.
7. F. M. Fowkes, in *Treatise on Adhesion and Adhesives* Ed. R. L. Patrick (Dekker, New York, 1967. Vol. 1, Chap. 9.
8. J. R. Dann, *J. Col. Interface Sci.* **32**, 321 (1970).
9. D. K. Owens, *J. Appl. Poly. Sci.* **14**, 1725 (1970).
10. A. N. Gent, and J. Schultz, *J. Adhesion* **3**, 281 (1972).
11. Orowan, *Fatigue and Fracture in Metals* (M.I.T. Symposium, June, 1950) (Wiley, New York, (1950).
12. J. C. Halpin, and H. W. Polley, *J. Comp. Matls.* **1**, 64 (1967).
13. J. C. Halpin, J. R. Kopf and W. Goldberg, *Ibid.* **4**, 462 (1970).
14. A. W. Neumann, and W. Tanner, Proc. 5th Int. Cong. on Surface Activity, Vol. 2 (1968), pp. 727–734.

15. G. Mozzo, and R. Chabord, Proc. 23rd Annual Conf., Reinforced Plastics/Composites Division, Soc. Plastics Industry, Section 9-C, (1968), pp. 1–8.
16. D. H. Kaelble, and E. H. Cirlin, *J. Poly. Sci., Part C* **35**, 79 (1971).
17. H. G. Tattersall, and G. Tappin, *J. Matl. Sci.* **1**, 296 (1966).
18. B. Harris, P. W. R. Beaumont and E. M. de Ferran, *Ibid.* **6**, 238 (1971).
19. W. A. Zisman, in *Adhesion and Cohesion* Ed. P. Weiss (Elsevier, Amsterdam 1962). p. 176.
20. A. H. Cottrell, *Proc. Roy. Soc.* **A282**, 2 (1964).
21. A. Kelley, *Ibid.* **A319**, 95 (1970).
22. D. H. Kaelble, *Trans. Soc. Rheol.* **15**, 275 (1971).
23. D. H. Kealble, *J. Macromol. Sci., Revs.–Macromol. Chem.* **C6**, 85 (1971).